JOURNAL OF AIRCRAFT
Vol. 31, No. 3, May–June 1994

Measured and Theoretical Supersonic Dynamic Stability Characteristics of a National Aero-Space Plane Configuration

David A. Dress,* Richmond P. Boyden,* and Christopher I. Cruz†
NASA Langley Research Center, Hampton, Virginia 23681

Wind-tunnel tests of a National Aero-Space Plane configuration were conducted in the NASA Langley Unitary Plan Wind Tunnel (UPWT). The model used is a Langley designed blended body configuration. Dynamic stability characteristics were measured on this configuration at Mach numbers of 2.0, 2.5, 3.5, and 4.5. In addition to tests of the baseline configuration, component breakdown tests were conducted. The test results show that the baseline configuration generally has stable damping about all three axes, with only isolated exceptions. In addition, there was generally good agreement between the in-phase dynamic parameters and the corresponding static data which were measured during another series of tests in UPWT. Also included are comparisons of the experimental damping parameters with results from the engineering predictive code aerodynamic preliminary analysis system. These comparisons show good agreement at low angles of attack; however, the comparisons are generally not as good at the higher angles of attack.

Nomenclature

The static and dynamic stability data presented are referred to the body axis system (inclined 4.25 deg relative to $WL = 0$) shown in Fig. 1. The dynamic stability balance and sting were offset 4.25 deg from the model centerline to avoid any alteration of the upper aft surface of the model. The origin of the axes was located to correspond to the moment reference position shown in Fig. 2. The model reference length for the pitching moment coefficients is the body reference length of 33.6 in. (see Fig. 2). For the yawing and rolling moment coefficients, the reference length is the overall wing span of 12.00 in. The reference area of 161.04 in.^{2} is the theoretical wing planform area (including elevons) with the wing leading edges projected to the centerline of the vehicle. The area of the body flap at the rear of the body and the canard are not included in the reference area.

b	= wing span, ft
C_l	= rolling-moment coefficient, (rolling moment/$q_\infty Sb$)
C_{l_p}	= $\frac{\partial C_l}{\partial(pb/2V)}$, per rad
$C_{l_{\dot p}}$	= $\frac{\partial C_l}{\partial(\dot p b^2/4V^2)}$, per rad
$C_{l_p} + C_{l_{\dot\beta}} \sin\alpha$	= damping-in-roll parameter, per rad
C_{l_β}	= $(\partial C_l/\partial\beta)$, per rad
$C_{l_{\dot\beta}}$	= $\frac{\partial C_l}{\partial(\dot\beta b/2V)}$, per rad
$C_{l_\beta} \sin\alpha - k^2 C_{l_{\dot p}}$	= rolling moment due to roll-displacement parameter, per rad
C_m	= pitching-moment coefficient, (pitching moment/$q_\infty SL$)
C_{m_q}	= $\frac{\partial C_m}{\partial(qL/2V)}$, per rad
$C_{m_{\dot q}}$	= $\frac{\partial C_m}{\partial(\dot q L^2/4V^2)}$, per rad
$C_{m_q} + C_{m_{\dot\alpha}}$	= damping-in-pitch parameter, per rad
C_{m_α}	= $(\partial C_m/\partial\alpha)$, per rad
$C_{m_{\dot\alpha}}$	= $\frac{\partial C_m}{\partial(\dot\alpha L/2V)}$, per rad
$C_{m_\alpha} - k^2 C_{m_{\dot q}}$	= oscillatory longitudinal-stability parameter, per rad
C_n	= yawing-moment coefficient, (yawing moment/$q_\infty Sb$)
C_{n_r}	= $\frac{\partial C_n}{\partial(rb/2V)}$, per rad
$C_{n_{\dot r}}$	= $\frac{\partial C_n}{\partial(\dot r b^2/4V^2)}$, per rad
$C_{n_r} - C_{n_{\dot\beta}} \cos\alpha$	= damping-in-yaw parameter, per rad
C_{n_β}	= $(\partial C_n/\partial\beta)$, per rad or deg
$C_{n_{\dot\beta}}$	= $\frac{\partial C_n}{\partial(\dot\beta b/2V)}$, per rad
$C_{n_\beta} \cos\alpha + k^2 C_{n_{\dot r}}$	= oscillatory directional-stability parameter, per rad
f	= frequency of oscillation, Hz
k	= reduced-frequency parameter, $(\omega L/2V)$ in pitch; $(\omega b/2V)$ in roll and yaw, rad
L	= body reference length, ft
M	= freestream Mach number
p	= angular velocity of model about X axis, rad/s
q	= angular velocity of model about Y axis, rad/s
q_∞	= freestream dynamic pressure, psf
r	= angular velocity of model about Z axis, rad/s
S	= reference area, ft^2
V	= freestream velocity, ft/s
WL	= water line
X, Y, Z	= dynamic stability body system of axes
α	= angle of attack, deg or rad
β	= angle of sideslip, deg or rad

Presented as Paper 92-5009 at the AIAA 4th International Aerospace Planes Conference, Orlando, FL, Dec. 1–4, 1992; received Feb. 8, 1993; revision received May 5, 1993; accepted for publication May 5, 1993.

*Aerospace Engineer, Supersonic/Hypersonic Aerodynamics Branch, Applied Aerodynamics Division, M/S 413. Senior Member AIAA.

†Aerospace Engineer, Vehicle Analysis Branch, Space Systems Division, M/S 365. Member AIAA.

ω = angular velocity, $2\pi f$, rad/s
$\cdot$ = indicates a first derivative with respect to time

Model Component Designations
B = body
N = nacelle
V = outboard vertical tails
W = wings

Introduction

As part of the development effort for the National Aero-Space Plane (NASP) program, a task was initiated at the Langley Research Center to measure experimentally the dynamic stability parameters of several configurations. Various configurations have been investigated during development of the NASP, including a cone body, blended body, fuselage/wing combination, and a waverider. These designs are uniquely shaped in order to meet their performance goals. In particular, the underside of the vehicle is generally integrated into the propulsion system.[1,2] These unique shapes, however, present problems in suitably mounting models of these designs for aerodynamic wind-tunnel tests. Specifically, there are concerns with the mounting system interfering with either the propulsion system's expansion ramp or the aft upper surface of these models. Therefore, the primary objective of this task was to develop and demonstrate high-speed dynamic stability test techniques for nonpowered NASP-type configurations. This small-amplitude, forced oscillation technique is labeled high-speed to distinguish it from similar low-speed techniques,[3] although this high-speed technique works equally well at subsonic, transonic, and supersonic speeds.

As a part of this task, supersonic dynamic stability results were measured for the Langley designed blended body configuration, designated the test techniques demonstrator (TTD). These results were acquired in the Langley Unitary Plan Wind Tunnel (UPWT)[4] at Mach numbers of 2.0, 2.5, 3.5, and 4.5. Some unpublished static results on the same model tested in the UPWT are included for comparison purposes. Component effects were obtained by testing with and without the wings, vertical tails, and nacelle. The range of angle of attack was from -2 to 18 deg. In addition to the test results, comparisons of the experimental damping parameters with results from the engineering predictive code aerodynamic preliminary analysis system (APAS)[5,6] are also included.

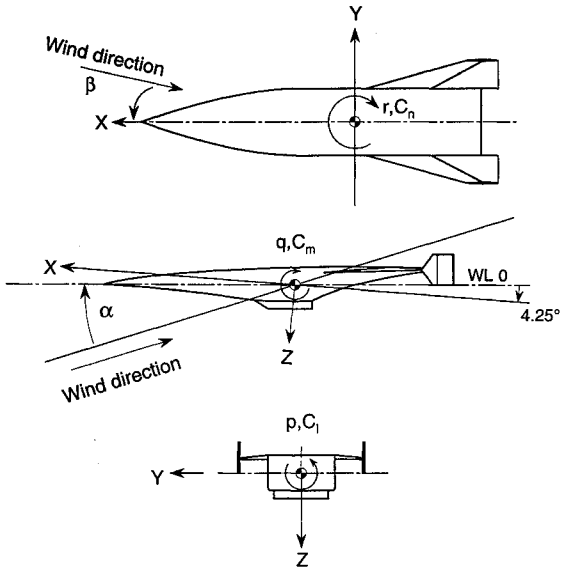

Fig. 1 System of axes used in investigation. Arrows indicate positive direction of moments, forces, and angles.

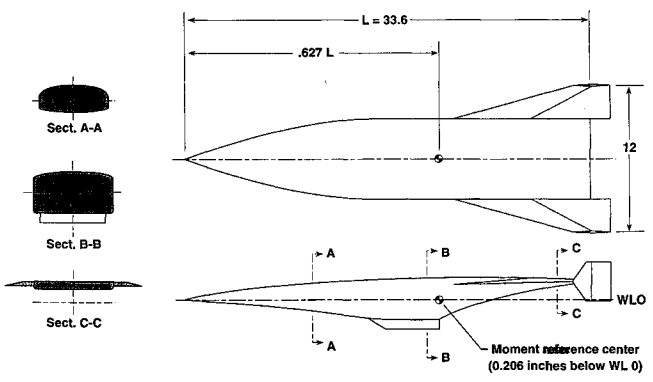

Fig. 2 Model geometry; linear dimensions are in inches.

Model and Apparatus

A sketch of the baseline TTD configuration is presented in Fig. 2. The wings have a 75-deg leading-edge sweep, an aspect ratio of 0.89, and a taper ratio of 0.13. The wings have a flat bottom with a half-diamond airfoil section on top. The half-diamond section is 3% thick with the maximum thickness at the 50% chord location. The wings are mounted 1.5-deg nose-down with respect to the fuselage reference line. The vertical tails have a 35-deg leading-edge sweep, an aspect ratio of 1.22, and a taper ratio of 0.65. These vertical tails have a diamond airfoil section with the maximum thickness varying linearly from 6% thick at the 25% chord location at the tip to 4% thick at the 50% chord location at the root. The vertical tails are also mounted at a -1.5-deg angle with respect to the fuselage reference line. The rectangular-shaped flow-through nacelle has a varying cross-sectional area along its length. The sidewalls of the nacelle at the inlet have a 60-deg leading-edge sweep. In addition, the sidewalls and the bottom wall at the inlet have 60-deg chamfers perpendicular to the leading edges.

Descriptions of the small-amplitude, forced oscillation dynamic stability technique and balances are given in Refs. 7 and 8.

Test Description

The tunnel total pressure was varied with the Mach number so that all of the data were taken at a constant Reynolds number per foot of 2.0 million. This corresponds to a stagnation pressure of 1254 psf for Mach 2.0, 1699 psf for Mach 2.5, 2882 psf for Mach 3.5, and 4666 psf for Mach 4.5. The total temperature of the airflow was held constant at 125°F for Mach 2.0 and at 150°F for the other Mach numbers, and the dew point was held below the minimum value at which condensation effects become significant.

At 2.0 Mach number, boundary-layer transition strips consisting of a 0.063-in. band of no. 50 grit were located 1.2 in. aft of the fuselage nose apex and 0.4 in. aft streamwise of the wing and vertical tail leading edges. The grit was applied to both surfaces of the wings and vertical tails. In the case of the nacelle, strips were applied 0.4 in. aft streamwise on the inside surfaces of the sidewalls and bottom wall. The chamfer located on the outside surfaces of the sidewalls and bottom wall precluded locating strips 0.4 in. aft streamwise. In this case, the strips were located just ahead of the downstream end of the chamfered surface. At the higher Mach numbers, single-spaced boundary-layer transition grit (no. 35) was applied at the same locations described above. Reference 9 was used to properly size the grit to provide fully turbulent flow over the model.

The forced-oscillation tests were conducted primarily to determine the pitch damping $C_{m_q} + C_{m_{\dot{\alpha}}}$, yaw damping $C_{n_r} - C_{n_{\dot{\beta}}} \cos \alpha$, and roll damping $C_{l_p} + C_{l_{\dot{\beta}}} \sin \alpha$ parameters. These parameters are all out-of-phase with the displacement of the oscillating model. The parameters in-phase with displacement are also measured. The in-phase parameters pre-

sented here are $C_{m_\alpha} - k^2 C_{m_{\dot{q}}}$, $C_{n_\beta} \cos \alpha + k^2 C_{n_{\dot{r}}}$, and $C_{l_\beta} \sin \alpha - k^2 C_{l_{\dot{p}}}$. A discussion of in-phase and out-of-phase parameters, as well as the data reduction procedure, is given in Ref. 7. For the pitch oscillation tests, the value of k varied from 0.0109 to 0.0267. During the yaw oscillation tests, k varied from 0.0041 to 0.0079, and for the roll oscillation tests, k varied from 0.0127 to 0.0232.

Experimental Results and Discussion

Pitching Characteristics

The oscillatory stability parameters measured during the pitching oscillation tests at Mach numbers of 2.0 and 4.5 are presented in Fig. 3. The upper portions of Figs. 3a and 3b show the results of component breakdown of the baseline configuration (BWVN) on the damping-in-pitch parameter. Negative values of the parameter represent stable damping in pitch. At 2.0 Mach number, all four configurations have mostly stable and essentially constant pitch damping over the angle-of-attack range, indicating that the main body of the model is dominant in determining the pitch damping for this configuration. There is an exception to this trend for the BN configuration where the damping increases significantly and unexpectedly between 10–14-deg angle of attack. At 4.5 Mach number, the trends are similar, but the damping level has decreased slightly through the angle-of-attack range. Instead of a sharp increase for the BN configuration at the higher angles of attack, there is an isolated peak in the damping at 10-deg angle of attack.

The lower portions of Figs. 3a and 3b show the oscillatory longitudinal-stability parameter results. The baseline configuration (BWVN) is stable at 2.0 Mach number up to an angle of attack of 6 deg. The effect of removing the wings is large as shown for the BN configuration, which is unstable through the angle-of-attack range at both 2.0 and 4.5 Mach numbers.

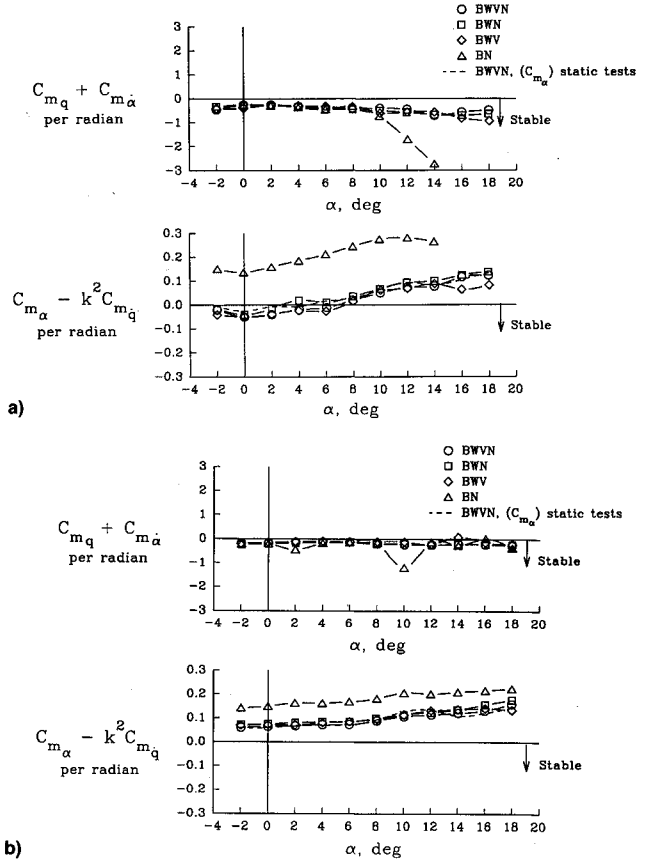

Fig. 3 Results of component breakdown of TTD configuration on the damping-in-pitch parameter and the oscillatory longitudinal-stability parameter: a) $M = 2.0$ and b) $M = 4.5$.

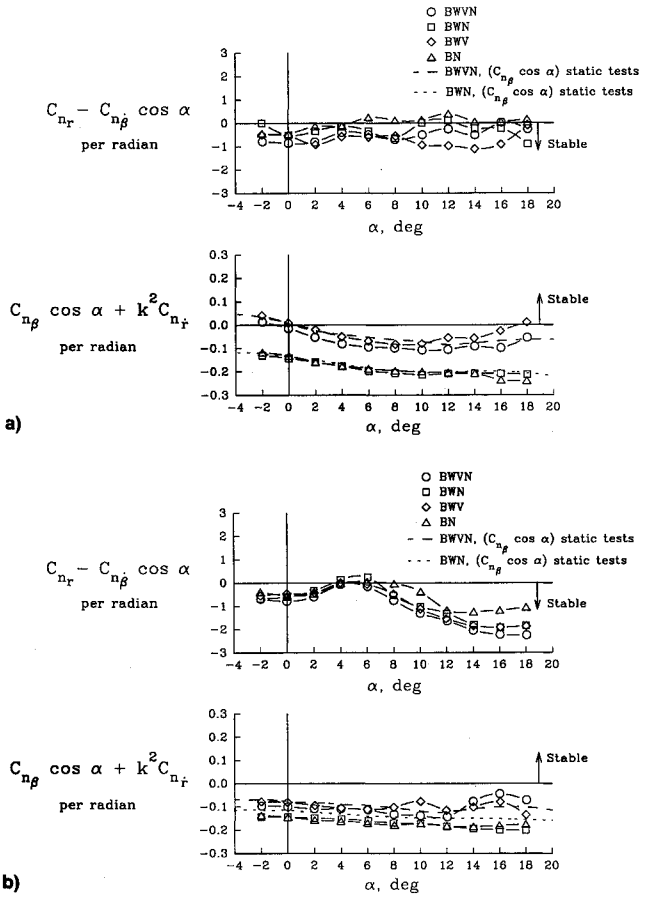

Fig. 4 Results of component breakdown of TTD configuration on the damping-in-yaw parameter and the oscillatory directional-stability parameter: a) $M = 2.0$ and b) $M = 4.5$.

At 4.5 Mach number, the baseline configuration is also unstable through the angle-of-attack range. In fact, the results at 4.5 Mach number for all configurations with wings have shifted upward into the unstable region, while the BN configuration results have remained at a fairly constant level. This is due to a loss of wing effectiveness with increasing Mach number. A comparison of C_{m_α} computed from the static test results with the oscillatory longitudinal-stability parameter is also shown in the lower portions of Figs. 3a and 3b. This comparison is for the baseline configuration and shows good agreement between the static and dynamic results, and thus indicates that, as expected, the $k^2 C_{m_{\dot{q}}}$ term is small in comparison to the C_{m_α} term. In addition, this good agreement gives confidence that the dynamic stability measurement technique is working properly. Note that comparisons between static and dynamic results are shown in Figs. 3–5. To make proper comparisons in these figures, the static data were transferred to the dynamic stability body axes and moment reference center.

Yawing Characteristics

The oscillatory stability parameters measured in the yawing oscillation tests are shown in Fig. 4 for Mach numbers of 2.0 and 4.5. The upper portions of Figs. 4a and 4b show the results of component breakdown of the baseline configuration (BWVN) on the damping-in-yaw parameter. At 2.0 Mach number the baseline configuration has stable damping in yaw (negative values of the parameter), except for near zero damping at 16-deg angle of attack. As expected, removing the outboard vertical tails (BWN configuration) generally decreases the damping level. Removing the wings and the outboard verticals from the baseline configuration generally decreases the damping even further. At 4.5 Mach number the trends are very different. In particular, there is a reduction in the damping level at 4–6-deg angle of attack, followed by a gradual in-

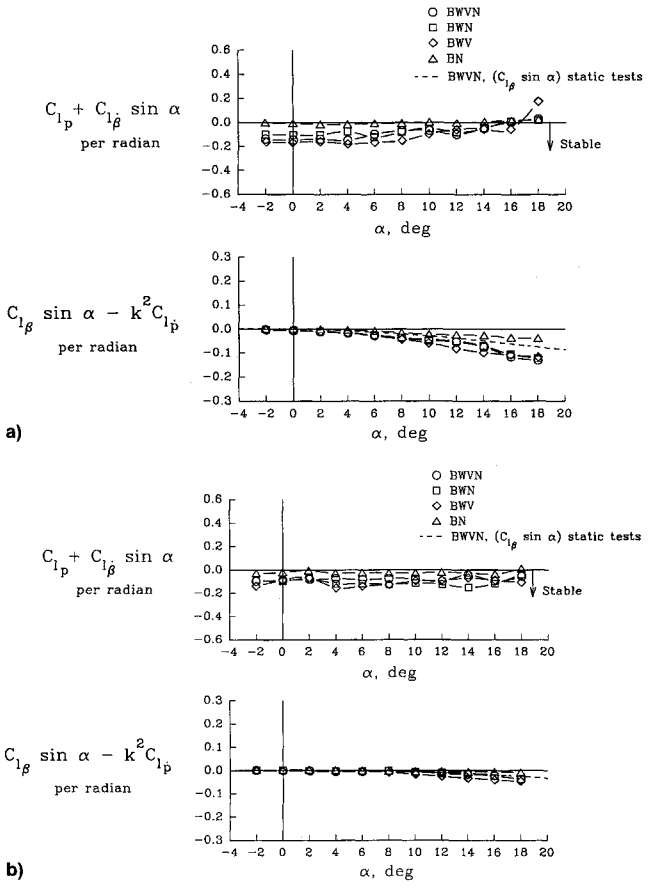

Fig. 5 Results of component breakdown of TTD configuration on the damping-in-roll parameter and the rolling moment due to roll displacement parameter: a) $M = 2.0$ and b) $M = 4.5$.

crease in the damping with increasing angle of attack. Despite the reduction, the baseline configuration has stable damping through the angle-of-attack range. Once again, removing the outboard vertical tails generally decreases the damping level, while removing the wings and the outboard verticals from the baseline configuration generally decreases the damping even further for angles of attack above 6 deg.

The lower portions of Figs. 4a and 4b contain the oscillatory directional-stability parameter results. At 2.0 Mach number for the baseline configuration, the directional-stability parameter has mostly negative values, indicating a destabilizing effect. As expected, removing the outboard vertical tails destabilizes the configuration even further, whereas removing the nacelle generally tends to stabilize the configuration since the nacelle is ahead of the model's c.g. At 4.5 Mach number, the results for the configurations with vertical tails (BWVN and BWV) have shifted further into the unstable region, while the results for the configurations without vertical tails have remained at a fairly constant level. This is due to a loss of vertical tail effectiveness with increasing Mach number. This effect was also measured on a conical aerospace plane configuration as discussed in Ref. 10. Also included in this figure is $C_{n_\beta} \cos \alpha$ computed from the static test results. Results are included for the baseline configuration and the baseline configuration with the vertical tails removed. For the baseline configuration at 2.0 Mach number, there is generally good agreement between the oscillatory directional-stability parameter and $C_{n_\beta} \cos \alpha$ computed from the static test results. At 4.5 Mach number, the agreement is good up to about 12 deg, and only fair at the higher angles of attack. In particular, the oscillatory directional-stability parameter is nonlinear above 12 deg. Recall that the dynamic results are based on a ±1-deg yaw oscillation amplitude, whereas the static results were obtained using $\beta = 3$ deg. Therefore, these differences may be due to the larger β value for the static results which may have missed a nonlinearity present at $\beta = 1$ deg. For the BWN configuration at 2.0 and 4.5 Mach numbers, there is good agreement between the oscillatory directional-stability parameter and $C_{n_\beta} \cos \alpha$ computed from the static test results.

Rolling Characteristics

The oscillatory stability parameters measured in the rolling oscillation tests are shown in Fig. 5 for Mach numbers of 2.0 and 4.5. The upper portions of Figs. 5a and 5b show the results of component breakdown of the baseline configuration (BWVN) on the damping-in-roll parameter. The baseline configuration generally has stable roll damping characteristics (negative values of the parameter) up to about 16 deg for 2.0 Mach number. Removing the outboard vertical tails or the nacelle from the baseline configuration generally has a very small effect on this parameter. Removing the wings and outboard vertical tails from the baseline configuration generally decreases the damping to the point where the BN configuration is neutrally damped through the angle-of-attack range. At 4.5 Mach number, the baseline configuration has stable roll damping through the angle-of-attack range. Again, the most significant effect of component breakdown is shown for the BN configuration, which has decreased damping through the angle-of-attack range.

For completeness, the bottom portions of Figs. 5a and 5b show the results of component breakdown of the baseline configuration on the rolling moment due to roll-displacement parameter, since this parameter was measured simultaneously with the damping-in-roll parameter. The first term in this parameter, $C_{l_\beta} \sin \alpha$, is the aerodynamic "spring" term resulting from the rolling motion about the body axis at angle of attack. Because of the "sin α" multiplier this parameter is not as useful as the effective-dihedral parameter.[7] However, the rolling moment due to roll-displacement parameter does serve to indicate gross effects such as a sign change in the dihedral effect. The effect of component breakdown on this parameter is minimal. The only change worth noting is a reduction in this parameter for the BN configuration at the higher angles of attack. These differences between the results for the baseline and the BN configurations decrease as Mach number increases. Data are also presented in Fig. 5 showing a comparison of this parameter and $C_{l_\beta} \sin \alpha$ computed from the static data. The comparison for the baseline configuration generally shows good agreement between the static and forced oscillation results. However, at 2.0 Mach number above 14 deg, the results do not agree due to a trend change in the dynamic data. The reason for the different trends at the higher angles of attack is unknown.

Data Uncertainty for the Damping Parameters

The data acquisition method used during these tests was based on sampling 40 filtered signal voltages for each channel at each data point for about 25 s. An arithmetic mean and standard deviation were calculated for each set of 40 signal voltages, and the arithmetic means were then used to calculate the aerodynamic parameters. Typically, two or three of these data points were taken for each test condition. Single aerodynamic parameter values at each test condition were achieved by calculating the arithmetic mean of the two or three aerodynamic parameter values. The standard deviations of these averaged aerodynamic parameters were also calculated at each test condition. This data acquisition procedure is used to minimize the effect of fluctuations of the signal voltage outputs caused by such things as separated flow on the model and unsteadiness of the tunnel flow.

Figure 6 gives a sample of data uncertainty for the baseline configuration by showing the damping-in-pitch parameter along with error bars representing plus or minus one standard deviation of this parameter. These error bars replace the symbols used in the preceding plots. In some cases, the standard deviation is so small that the error bars blend in with the line or the standard deviation is less than 0.00005, in which case

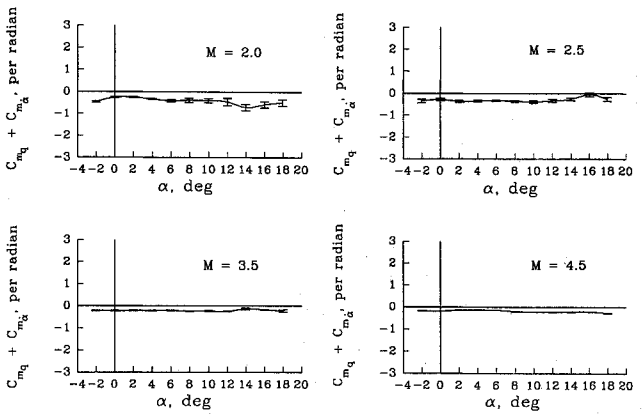

Fig. 6 Sample of measurement uncertainties for the damping-in-pitch parameter for the baseline configuration.

the deviation is assumed to be negligible and error bars are not shown. Figure 6 shows that the uncertainty of this parameter decreases as Mach number increases from 2.0 to 4.5. In addition, at 2.0 Mach number, the uncertainty generally increases with increasing angle of attack.

APAS Description

The APAS is an interactive computer program which allows an experienced user to quickly estimate aerodynamic forces and moments of arbitrary aerospace vehicles. Once the analysis geometry has been defined, a low-speed or high-speed analysis module is executed to perform the aerodynamic force and moment estimations. For the comparisons in this article, the high-speed analysis module was used. In this module, a noninterference finite surface element model of the vehicle is analyzed using empirical impact pressure and approximate skin friction methods. This high-speed or supersonic/hypersonic analysis module of APAS is an enhanced version of the Hypersonic Arbitrary Body Program Mark III (HABP3). Detailed information concerning APAS, including program formulation and comparisons with experimental data and CFD results, can be found in Refs. 5 and 6, and 11–15.

APAS Analysis of the TTD

The supersonic/hypersonic analysis module of APAS was used to estimate damping derivatives (C_{mq}, C_{nr}, and C_{lp}) for the baseline configuration (BWVN) and the body-nacelle configuration (BN). Figure 7 illustrates the TTD as modeled and analyzed. At each tunnel condition, four separate APAS analyses were performed (one analysis with no vehicle rotation, and one each with p, q, and r, equal to one rad/s). The APAS recommended default methods for surface pressure estimation were utilized. They included the tangent-cone approximation for the body surface and the tangent-wedge approximation for the nacelle, wings, and outboard vertical tail surfaces. The rotation rates p, q, and r, entered the APAS calculation process as local velocity increments. The moment increments used in calculating the dynamic damping derivatives were then calculated by differencing two APAS results (one with a one rad/s rotation and one with no vehicle rotation).

Comparison of APAS Results with Wind-Tunnel Data

The results of APAS comparisons with the wind-tunnel data are shown in Figs. 8–10. Note that APAS can estimate only the first of the two combined terms in each of the damping parameters. For the baseline configuration, there was better agreement for the damping-in-pitch parameter than for either the damping-in-yaw or damping-in-roll parameters. This is also true for the BN configuration for angles of attack up to about 10 deg. Generally, good agreement was shown between APAS results and the wind-tunnel data for both the baseline and the BN configurations at low angles of attack (−2 deg

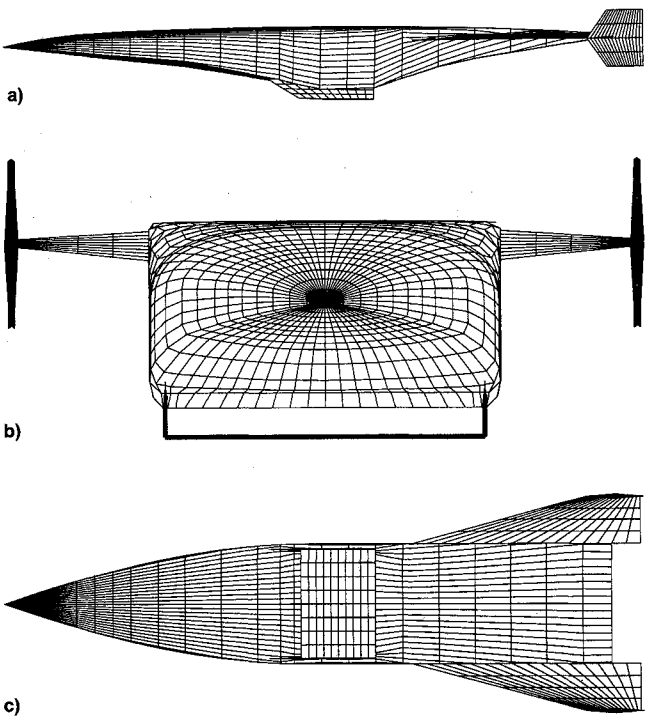

Fig. 7 APAS model of baseline TTD configuration: a) side view, b) frontal view, and c) bottom view.

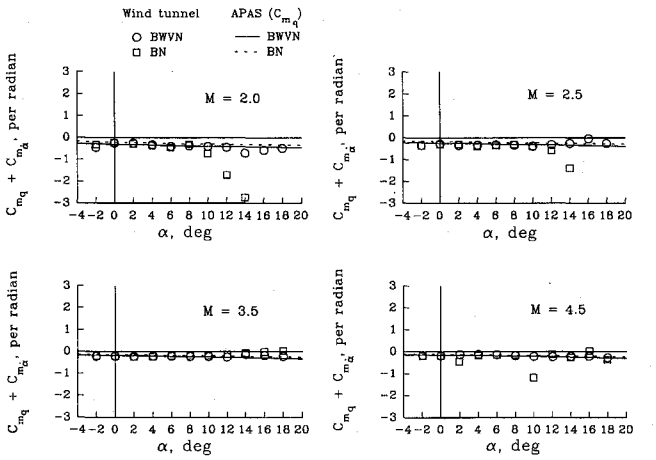

Fig. 8 Comparison of APAS results with damping-in-pitch parameter.

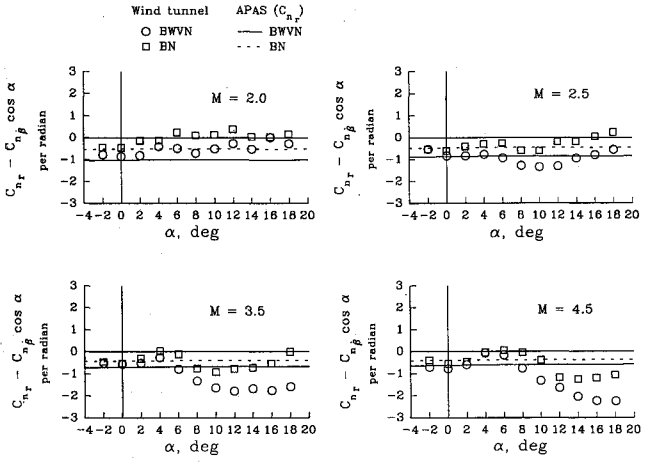

Fig. 9 Comparison of APAS results with damping-in-yaw parameter.

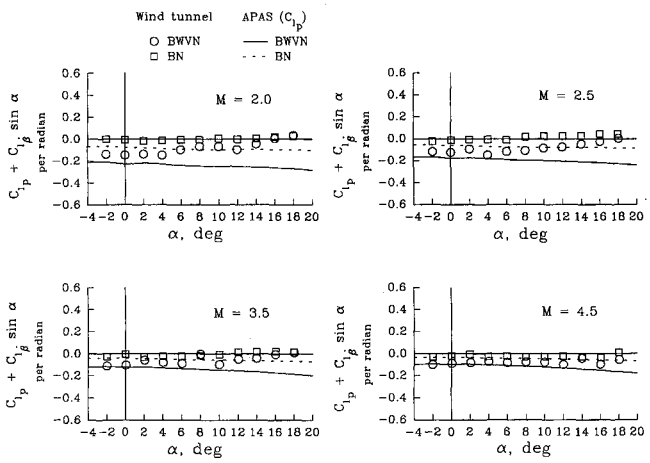

Fig. 10 Comparison of APAS results with damping-in-roll parameter.

$< \alpha < 6$ deg). As angle of attack increases, agreement between the APAS results and the wind-tunnel data was generally not as good. There are two possible reasons for this angle-of-attack trend. The first can be explained in a qualitative sense by looking closely at the calculation procedure in the high-speed module of APAS. First, APAS divides the vehicle surface into quadrilateral elements. Next, the surface pressure coefficient and local skin friction coefficient on each panel are estimated independent of the presence of the rest of the panels which make up the configuration. For example, a body surface element whose tangent vector is inclined by 5 deg from the freestream velocity vector is assumed to have the surface properties associated with a sharp, 5-deg cone at 0-deg angle of attack at the specified analysis conditions. The fact that this surface element may be located downstream of the nose of the body and/or the wing leading edge is neglected. Thus, as angle of attack increases, an increasing deviation between APAS estimates and wind-tunnel data is not surprising. The second possible reason for the less favorable comparisons at the higher angles of attack is the fact that APAS does not estimate the second of the two combined terms (either the $\dot{\alpha}$ or $\dot{\beta}$ terms) in each of the damping parameters. As shown in Refs. 11–15, however, good agreement between APAS results and static wind-tunnel data is often encountered throughout the angle-of-attack range.

Summary of Results

The small-amplitude, forced-oscillation dynamic stability technique was successfully used to test a nonpowered NASP configuration in the pitch, yaw, and roll modes. In particular, this investigation was conducted to determine the supersonic dynamic stability characteristics of a Langley designed blended body configuration designated the TTD. These tests were made over a range of Mach numbers from 2.0 to 4.5, and over a range of angles of attack from −2 to 18 deg. The results are summarized as follows:

1) For both the longitudinal and lateral-directional data there was generally good agreement between the in-phase dynamic parameters and the corresponding static data.

2) The baseline configuration generally has stable damping about all three axes with only isolated exceptions.

3) The measurement uncertainties for the damping parameters are generally small and decrease with increasing Mach number.

4) There is generally good agreement between the APAS results and the wind-tunnel data at low angles of attack (-2 deg $< \alpha < 6$ deg). As angle of attack increases, the agreement was generally not as good.

References

[1]Harris, R. V., Jr., "On the Threshold—The Outlook for Supersonic and Hypersonic Aircraft," AIAA Paper 89-2071, July–Aug. 1989.

[2]Sanchez, F., "The National Aero-Space Plane, the Guidance and Control Engineer's Dream or Nightmare? Guidance and Control 1989," *Proceedings of the Annual Rocky Mountain Guidance and Control Conference*, Keystone, CO, Feb. 1989; see also Advances in the Astronautical Science, Vol. 68, AAS 89-040, Feb. 1989, pp. 339–352.

[3]Chambers, J. R., and Grafton, S. B., "Investigation of Lateral-Directional Dynamic Stability of a Tilt-Wing V/STOL Transport," NASA TN D-5637, Feb. 1970.

[4]Jackson, C. M., Jr., Corlett, W. A., and Monta, W. J., "Description and Calibration of the Langley Unitary Plan Wind Tunnel," NASA TP-1905, Nov. 1981.

[5]Bonner, E., Clever, W., and Dunn, K., "Aerodynamic Preliminary Analysis System II. Part I—Theory," NASA CR-182076, April 1991.

[6]Sova, G., and Divan, P., "Aerodynamic Preliminary Analysis System II. Part II—User's Manual," NASA CR-182077, April 1991.

[7]Freeman, D. C., Boyden, R. P., and Davenport, E. E., "Supersonic Dynamic Stability Characteristics of a Space Shuttle Orbiter," NASA TN D-8043, Jan. 1976.

[8]Braslow, A. L., Wiley, H. G., and Lee, C. Q., "A Rigidly Forced Oscillation System for Measuring Dynamic-Stability Parameters in Transonic and Supersonic Wind Tunnels," NASA TN D-1231, March 1962 (supersedes NACA RM L58A28).

[9]Braslow, A. L., and Knox, E. C., "Simplified Method for Determination of Critical Height of Distributed Roughness Particles for Boundary-Layer Transition at Mach Numbers from 0 to 5," NACA TN-4363, Sept. 1958.

[10]Hahne, D. E., Luckring, J. M., Covell, P. F., Phillips, W. P., Gatlin, G. M., Shaughnessy, J. D., and Nguyen, L. T., "Stability Characteristics of a Conical Aerospace Plane Concept," Society of Automotive Engineers 892313, Sept. 1989.

[11]Cruz, C., and Wilhite, A., "Prediction of High-Speed Aerodynamic Characteristics Using the Aerodynamic Preliminary Analysis System (APAS)," AIAA Paper 89-2173, July–Aug. 1989.

[12]McCandless, R., and Cruz, C., "Hypersonic Characteristics of an Advanced Aerospace Plane," AIAA Paper 85-0346, Jan. 1985.

[13]Blosser, M., Scotti, S., Cerro, J., Powell, R., Jackson, L. R., and Cruz, C., "Design Study of a Slant-Nose-Cylinder Aeroassisted Transfer Vehicle," AIAA Paper 85-0966, June 1985.

[14]Phillips, W. P., and Cruz, C., "Super/Hypersonic Aerodynamic Characteristics for a Transatmospheric Vehicle Concept Having a Minimum Drag Forebody," AIAA Paper 91-1694, June 1991.

[15]Cruz, C., and Ware, G., "Predicted Aerodynamic Characteristics for HL-20 Lifting-Body Using the Aerodynamic Preliminary Analysis System (APAS)," AIAA Paper 92-3941, July 1992.